Femtosecond structural probing of warm dense matter with Betatron x-ray source

Fabien Dorchies, Adrïan Grolleau, Sylvain Briand, Julien Gautier, Patrick Renaudin, Vanina Recoules, Kim Ta Phuoc, Ludovic Lecherbourg

PROCEEDINGS OF SPIE

SPIEDigitalLibrary.org/conference-proceedings-of-spie

Femtosecond structural probing of warm dense matter with Betatron x-ray source

Fabien Dorchies, Adrïan Grolleau, Sylvain Briand, Julien Gautier, Patrick Renaudin, et al.

Fabien Dorchies, Adrïan Grolleau, Sylvain Briand, Julien Gautier, Patrick Renaudin, Vanina Recoules, Kim Ta Phuoc, Ludovic Lecherbourg, "Femtosecond structural probing of warm dense matter with Betatron x-ray source," Proc. SPIE 12582, Compact Radiation Sources from EUV to Gamma-rays: Development and Applications, 125820A (8 June 2023); doi: 10.1117/12.2665807

SPIE.

Event: SPIE Optics + Optoelectronics, 2023, Prague, Czech Republic

Femtosecond structural probing of warm dense matter with Betatron x-ray source

Fabien Dorchies*[a], Adrïan Grolleau[b], Sylvain Briand[a,b], Julien Gautier[c], Patrick Renaudin[b], Vanina Recoules[b], Kim Ta Phuoc[c], Ludovic Lecherbourg[b,c]
[a]Univ. Bordeaux, CNRS, CEA, CELIA, UMR 5107, F-33400 Talence, France
[b]CEA, DAM, DIF, F-91297 Arpajon, France
[c]LOA, ENSTA, CNRS, Ecole Polytechnique, UMR 7639, F-91761 Palaiseau, France

ABSTRACT

Exploring and understanding ultrafast processes at the atomic level is a scientific challenge. Femtosecond X-ray Absorption Near-Edge Spectroscopy (XANES) arises as an essential experimental probing method, as it can simultaneously reveal both electronic and atomic structures, and thus potentially unravel their non-equilibrium dynamic interplay which is at the origin of most of the ultrafast mechanisms. The key point of this investigation is the achievement of a femtosecond X-ray source suitable for routine experiments. This paper will show the progressive development and improvement of such laser-plasma-based X-ray sources, starting from the picosecond down to the femtosecond scale. Time-resolved XANES measurements have been achieved and interpreted using ab initio quantum molecular dynamics simulations. This diagnostic was used to shed new light on the non-equilibrium physics involved in various materials. This paper will focus on results devoted to the non-equilibrium dynamics of a copper foil brought from solid to warm dense matter regime, by the use of a femtosecond laser pulse. Particular emphasis will be given to the recent study of the ultrafast electronic transport, which was revealed by the femtosecond time resolution.

Keywords: Ultrafast X-ray science, high energy density, phase transitions, time-resolved XANES

1. INTRODUCTION

This work is part of a long-term effort to develop time-resolved X-ray Absorption Near-Edge Spectroscopy (XANES) for the investigation of Warm Dense Matter (WDM) [1]. Such an extreme regime of matter, at the frontier between solid state and plasma physics (temperature up to a few 10 000 K, and density close to the solid density) can be transiently achieved using different experimental techniques. As strong correlations are expected in this dense regime, the use of XANES is supposed to provide valuable information concerning atomic and electronic structures, as it is the case in condensed matter, and to reveal their dynamical interplay.

An inexpensive way (in terms of energy invested) to produce WDM in the laboratory, is to use the isochoric heating of a thin foil by a femtosecond laser pulse. That creates a non-equilibrium situation for a few picoseconds, where the temperature of the electrons exceeds the one of ions. This process involves several mechanisms with various time scales, such as electron heating and transport, electron-ion coupling, phase transitions and hydrodynamic expansion. In order to investigate their respective dynamics, we have developed time-resolved XANES experiments with a progressive improvement of the resolution from a few picoseconds down to femtosecond [2 – 5]. In this paper, we illustrate these developments by presenting a series of experimental campaigns carried out on different laser systems, all concerning the study of the femtosecond heating of warm dense copper [5 – 8].

The first section will summarize the work performed, both on the theoretical side to interpret the different XANES features [9], and on the experimental one to resolve the picosecond dynamics of the two temperatures system. Most of this paper will then be devoted to the recent demonstration of femtosecond XANES with a Betatron x-ray source [5]. It allowed us to access the physics of the very first moments after the laser energy deposition, and in particular to investigate the ultrafast electronic transport in depth of the copper sample [8].

*fabien.dorchies@u-bordeaux.fr

Compact Radiation Sources from EUV to Gamma-rays: Development and Applications,
edited by Carmen S. Menoni, Jaroslav Nejdl, Proc. of SPIE Vol. 12582, 125820A
 · 0277-786X · doi: 10.1117/12.2665807

2. TWO TEMPERATURE WARM DENSE COPPER INVESTIGATION AT THE PICOSECOND SCALE

2.1 Two temperature hydrodynamic simulations

The Two-Temperature Model (TTM) has been proposed to predict the electron-ion dynamics at the macroscopic scale [10]. Both sub-systems are there described by their respective temperature T_e (electrons) and T_i (ions). And their dynamic interplay is derived from a set of two differential equations (considering below one spatial dimension corresponding to the sample depth).

$$C_e \partial_t T_e = - G_{ei} (T_e - T_i) + \partial_x(\kappa_e \partial_x T_e) + S \quad (1)$$

$$C_i \partial_t T_i = G_{ei} (T_e - T_i) + \partial_x(\kappa_i \partial_x T_i) \quad (2)$$

S is the source term (energy deposited in the electrons). The physics is governed by the heat capacities C_e and C_i, the heat conductions κ_e and κ_i, and the electron-ion coupling parameter G_{ei}. These parameters (especially C_e, κ_e and G_{ei}) can be calculated as a function of T_e from solid-state assumptions [11], or from first-principles calculations [12]. This simple model has been consistently integrated in the one-dimensional hydrodynamics code ESTHER [13], in which the hydrodynamic expansion is driven by an equation of state. This combination gives the thermodynamic evolution of the sample, that is to say of the electron and ion temperatures and the density.

The phase transitions can be predicted by a "thermal" approach, considering that they occur as soon as the appropriate thermodynamic conditions are satisfied. For example, the melting would take place when T_i exceeds the melting temperature. In some strong out-of-equilibrium situations, more exotic phenomena are expected. In covalent materials, electronically driven phase transitions were reported, also referred to as nonthermal melting [14]. In metals, depending on the nature of the electronic density of state (e.g. full *d*-band metals such as Cu, Ag or Au), the strongly excited electron system could cause lattice strengthening [15] also referred to as bond hardening [16]. This is what motivated us to study the femtosecond heating of warm dense copper. An example of two-temperature calculation in copper is plotted in the figure 1.

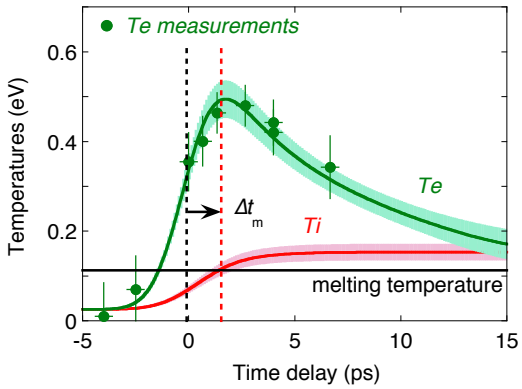

Figure 1. Time evolution of electron (T_e) and ion (T_i) temperatures estimated with two-temperature hydrodynamic simulations, and compared with T_e measurements, when 0.065 J/cm^2 is absorbed in a 80 nm copper foil. Calculations have been convoluted with the experimental time instrumental response. *Figure taken from ref [7].*

2.2 L3-edge XANES features interpretation using DFT-MD calculations

The fast transition from solid to warm dense copper has been investigated with time-resolved XANES, near the L3-edge located at 932.5 eV. In principle, this diagnostic probes the electronic structure near the continuum. More specifically, it probes the unoccupied *d*-states from the $2p_{3/2}$ core level. In this way, it may provide information about the modification of the 3*d*-band which dominates most of the macroscopic properties of copper. On the other hand, since the electronic band structure depends on the crystalline order, one may expect additional information about the atomic structure. The XANES interpretation is very specific to the material considered. Many calculations have been computed in solid-state physics, but a specific methodology is needed for disordered systems.

We carried out simulations using molecular dynamics based on the Density Functional Theory (DFT). Details are given in the reference [9]. Ionic configurations are computed for a set of given thermodynamic conditions (T_e, T_i, and the density ρ). Then, a more detailed electronic structure calculation is performed, in order to compute the x-ray absorption cross-section. This methodology to compute XANES spectra for two-temperature warm dense matter has been validated on a wide variety of systems and DFT molecular dynamics is now a powerful tool to support the interpretation of XANES measurements in WDM [1].

Some calculations are plotted in the figure 2. At solid state (black curve), the copper L3-edge is located at 932.5 eV, and followed by some modulations (post-edge). These are characteristic from the crystalline order (here fcc). Calculations demonstrate that they vanish when the lattice periodicity is lost. A pre-edge feature appears when the electron temperature T_e increases. The amplitude and shape of the pre-edge is directly linked to the modification of the 3*d* electronic population, as electronic states below the Fermi level deplete in favor of states above this level. The spectral integral of this pre-edge (with respect to the cold spectrum) can be used to deduce T_e for a wide range of temperatures and densities, as illustrated in the right part of the figure 2.

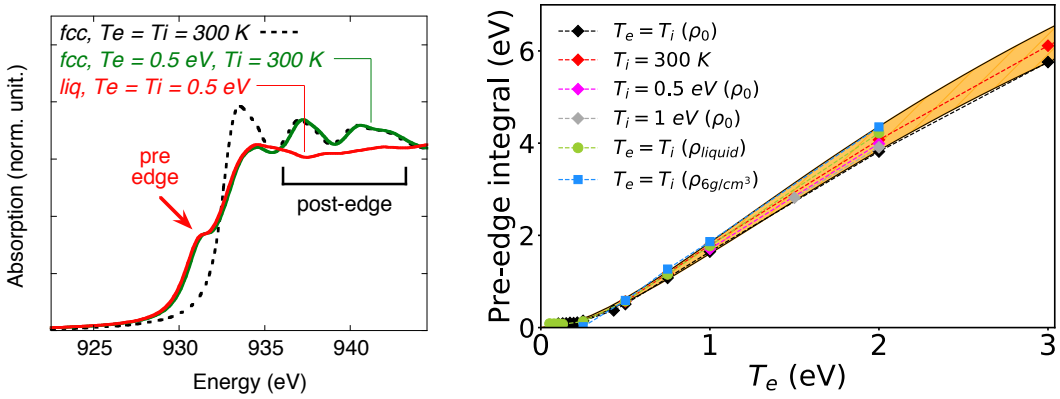

Figure 2. XANES spectra calculations at the L3-edge of copper (932.5 eV). Left: a pre-edge feature appears when the electron temperature T_e exceeds ~ 0.25 eV, while post-edge modulations are characteristic of the crystalline order (fcc). *Figure taken from ref [7]*. Right: evolution of the pre-edge integral as a function of T_e, calculated with different conditions for T_i and density (ρ). *Figure taken from ref [9].*

2.3 Experimental studies at the picosecond scale: electron – ion thermal equilibration and ultrafast melting

First series of experimental campaigns have been carried out with the help of the XANES station at the CELIA laboratory, fully described in the reference [4]. The measurements were recorded in a pump (femtosecond laser) – probe (picosecond x-ray pulse) scheme. The x-ray source originates from the M-shell thermal emission of a plasma produced in the laser interaction with a high *Z* dense target. Such emission exhibits bright and broadband spectra that can be adjusted with the target material. Considering the energy of the copper L3-edge, we considered the M-shell emission from a CsI solid target and a Xe cluster jet. The use of Xe clusters decreased the time resolution down to 1.2 ± 0.2 ps [17].

Some XANES spectra measured at different delays with respect to the laser heating, are plotted in the left part of the figure 3. Each spectrum is the result of the accumulation of ~ 100 shots. Note that the copper sample is shifted after each shot, since the heated area is destroyed by the pump beam. On the figure, we clearly see that the pre-edge increases rapidly after heating, then gradually decreases on a longer time scale. Using the demonstrated relation between the pre-edge and T_e (see the right part of figure 2), we retrieved the time evolution of the electronic temperature for a wide range of laser fluences. One example is plotted in the right part of the figure 3 (with 0.4 J/cm^2 absorbed). The rise time of T_e is limited by the instrumental picosecond resolution, but the following decrease extends over ~ 10 ps. It corresponds to the thermal equilibration from electrons to ions.

Data have been compared with two-temperature hydrodynamics simulations performed with different sets of parameters (see sub-section 2.1 and the equations therein). The best agreement was found when considering T_e-dependent parameters, whether they come from solid-state assumptions [11], or from first-principles calculations. Indeed, in this regime, the differences are slight because the electron 3*d*-band shape is not significantly modified when the solid copper turns to

WDM. At the longest delays (and at this highest laser fluence investigated), the hydrodynamic expansion contributes to further reduce T_e, even after the electron-ion thermal equilibration, since some energy is converted into kinetic energy.

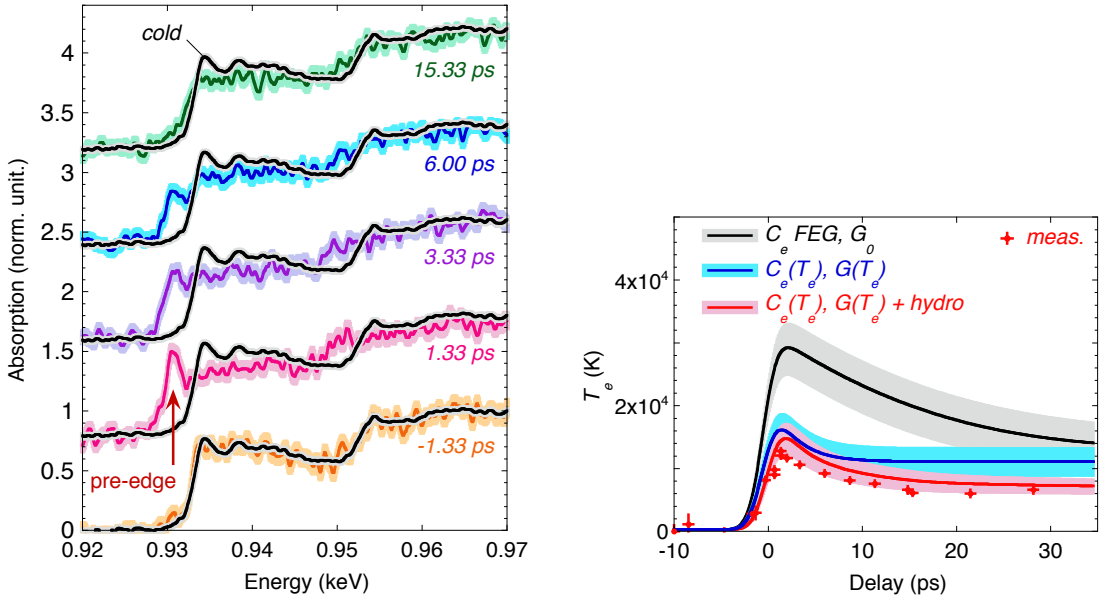

Figure 3. Left: some time-resolved XANES spectra recorded when 0.4 J/cm^2 is absorbed in a 80 nm copper foil. Right: time evolution of T_e retrieved from pre-edge measurements, and compared with different two-temperature calculations. *Figures taken from ref [6].*

By respecting a rigorous protocol for the data acquisition and analysis, the signal-to-noise ratio was limited by the statistics of x-ray photon counting on the detector [4]. Therefore, it could be improved by increasing the number of shots. By accumulating ~ 1000 shots per spectrum, we were able to resolve the time evolution of the post-edge features, as illustrated in the left part of the figure 4. The spectrum registered 1.3 ps after heating (green) shows a clear non-equilibrium situation, where the lattice is still cold (fcc as demonstrated by the unchanged post-edge features) while the electron temperature is high (about 0.5 eV as retrieved from the pre-edge level).

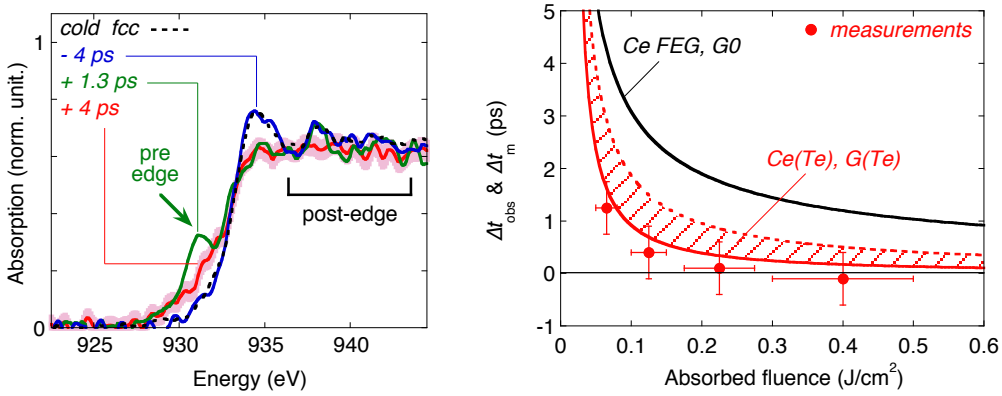

Figure 4. Left: some time-resolved XANES spectra recorded when 0.065 J/cm^2 is absorbed in a 80 nm copper foil. Right: time delay Δt_{obs} measured for the transition from fcc to liquid, compared with calculated melting time Δt_m, as a function of the absorbed laser fluence. *Figures taken from ref [7].*

From these measurements, we inferred the time Δt_{obs} needed for the crystalline order to disappear. The comparison with the calculated melting time Δt_m is plotted in the right part of the figure 4. Again, a good agreement is observed when T_e-

dependent parameters are considered in the two-temperature model, and this in a wide range of absorbed laser fluence (up to 0.4 J/cm^2, corresponding to a maximal temperature calculated of ~ 2 eV just after heating). Data do not indicate any bond hardening effect, which is not surprising since this effect has been predicted for $T_e \geq 3$ eV [15].

2.4 Femtosecond XANES demonstration with Betatron x-ray source

As demonstrated above, a picosecond time resolution provides access to a rich physics, but it is mandatory to reach down the femtosecond scale in order to reveal other ultrafast mechanisms. For example, the investigation of possible bond hardening requires higher laser flux, for which the melting is expected to be very fast (see the right part of the figure 4). We chose to use the Betatron radiation [18] which presents unique characteristics for femtosecond XANES: very short duration (~ 10 fs), broadband and shot-to-shot stable spectrum, and compatibility with table-top laser systems.

A specific set-up has been coupled to the Betatron source at the LOA laboratory. Details are given in the reference [5]. A special shielding and automation effort was made in order to get rid of the noise induced by undesirable hard x-ray photons. Some copper L3-edge XANES spectra will be plotted in the next section, after accumulation of ~ 100 laser shots (figure 6). Due to the number of x-ray photons registered on the detector, the signal-to-noise ratio is a bit lower than previously reported in the figure 3. But it is high enough to resolved the pre-edge, then to determine the electron temperature T_e as a function of the delay with respect to the heating laser pulse. First results reported in the reference [5] indicate a time resolution below 75 ± 25 fs. This demonstration experiment opens the paths for studying matter under extreme conditions, as well as ultrafast science in general.

3. FEMTOSECOND RESOLUTION OF THE ELECTRON ENERGY TRANSPORT IN WARM DENSE COPPER

This achievement was used for the investigation of the ultrafast laser heating and electronic transport in the depth of the copper sample. The time required to get homogeneous heated sample had been neglected so far, because of the picosecond time resolution and the limited laser flux.

3.1 Electron transport issue at high flux

The key point to study the warm dense matter regime is to be ensured to probe a relatively homogeneous slab of material in terms of temperatures and density. In the past, most femtosecond laser experiments invoked the ballistic transport of electrons in solid targets to justify the ultrafast and homogeneous heating of thin metal foils, for laser flux below 10^{13} W/cm² [7,16,19-22]. Ballistics electrons are non-thermal, and propagate through a sample with a ballistic motion, heating the in-depth electrons by collisions over a characteristic distance called the mean free path (MFP). In 2012, Z. Chen and coworkers performed an experiment using a chirped pulse to measure single-shot time-resolved optical reflectivity of both sides of a 30 nm thick laser heated gold sample [23]. They have highlighted an absorbed laser flux limit Q_{NT} for the ballistic electron transport, that can be understood using a phenomenological model (eq. 3). In this model, the flux evacuated by the ballistic electrons is limited by the maximum density of charge carriers in the material (assumed to be the free-electron density n_e), the maximum energy an electron can transport ballistically (assimilated to the Fermi energy E_F) and the maximum speed of the ballistic electrons (assumed to be the Fermi speed v_F).

$$Q_{NT} = n_e E_F v_F \tag{3}$$

The predicted Q_{NT} for gold of 7.3×10^{12} W/cm² is very close to the experimental value determined by Chen and coworkers. Above this value, they suggested that diffusive transport should gradually take over the ballistic transport, and induce an inhomogeneous heating. The study of the electron transport dynamics was still to be performed in the femtosecond regime, as their ~500 fs time resolution was not sufficient to investigate electron dynamics during the first picosecond of the heating.

3.2 Methodology

To investigate the electron energy transport, we performed an optical pump – x-ray probe experiment with femtosecond resolution on warm dense copper. 100 nm and 30 nm thick copper films deposited on 1 µm Mylar substrate have been heated above the ballistic flux limit, and XANES spectra were measured for different pump-probe delays near the copper L3 edge. The principle is schemed on figure 5. A 800 nm, 30 fs “pump” laser pulse was focused on a copper sample, 2.2°

incidence from the normal, to obtain an absorbed laser flux above the flux limit Q_{NT}. The laser energy is deposited in the skin depth of 13 nm [24], then transported deeper.

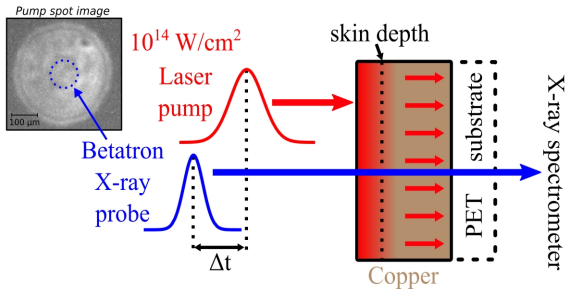

Figure 5. Principle of the pump-probe experiment. A laser heated copper film is probed by a femtosecond betatron x-ray pulse to diagnose the average electron temperature of the sample, giving access to the electron energy transport from the energy reservoir (skin depth) through the entire thickness of the sample. *Figure taken from ref. [8].*

For copper, using $n_e = 8.49\text{x}10^{22}$ cm^{-3}, $E_F = 7.04$ eV and $v_F = 1.57\text{x}10^8$ cm/s (from Ashcroft [25]), $Q_{NT} = 1.5\text{x}10^{13}$ W/cm². The pump laser fluence was (3.3 ± 0.9) J/cm². We managed to measure the sample reflectivity, and then deduce the absorbed laser flux $Q_{abs} = (2.5 \pm 0.7)\ \text{x}10^{13}$ W/cm², so that $Q_{NT} = 0.6\text{x}Q_{abs}$. The uncertainty on the flux is mainly due to the spatial inhomogeneity rather than shot-to-shot fluctuations. In this configuration, according to Chen model, 60% of the electron energy should be transported ballistically, and 40% by thermal diffusion. The mean free path of the ballistic electrons in copper is approximately 70 nm [26]. Two sample thicknesses have been used: 30 nm, close to the skin depth and thinner than the electron MFP, in which an homogeneous heating is expected, and 100 nm, in which the dynamics of the electron temperature has been investigated during the energy transport.

The betatron x-ray pulse was focused on the copper sample at normal incidence, using a gold plated toroidal mirror at 2° grazing incidence, giving a ~150 µm spot diameter. The x-ray spectra were recorded on a charge-coupled device (CCD) camera coupled with a Rubidium Acid Phtalate (RbAP) cylindrical crystal in the Johann configuration. The spectral calibration is done by identifying the Cu L3 and L2 edges at 932.5 eV and 952.5 eV respectively. The theoretical time resolution of such setup is ~40 fs, given by the quadratic sum of the pump duration (30 fs), the geometric contribution of the 2.2° pump-probe angle (~20 fs difference between the extreme parts of the probed area) and the betatron theoretical duration (10 fs), and experimentally demonstrated better than (75 ± 25) fs [5]. This value has been validated with the results on the 30 nm samples (see in part 3.3).

Images on the CCD camera were acquired by series of 100 successive shots (0.2 Hz shot rate), conducting to stacks composed of 100 images each. A XANES spectra is the result of 100 reference shots without the copper sample compared to 100 shots with the sample, cold, or heated at different pump-probe delays. Each spectrum is built in ~20 minutes, and around 100 spectra were obtained for a total of approximately 20000 shots during the experiment. It was made possible thanks to the betatron shot-to-shot stability and a fully automated acquisition sequence. Hot spots on the images, due to high energy x-rays and particles, are important contributors to the signal-to-noise ratio (SNR). As they are stochastic by nature, it was possible to remove them digitally thanks to a specific numerical procedure, using the whole 100 images of a given stack, in which the x-ray signal of interest is considered to be systematic, and the hot spots random events. The uncertainty on XANES spectra is then mainly due to the photon counting statistics.

3.3 Femtosecond XANES measurements

Examples of recorded XANES spectra for 100 nm thick copper are shown in the left part of figure 6. Below the L3 edge at 932.5 eV, a large pre-edge structure grows rapidly in approximately 1 ps. Using the pre-edge integral dependency on the electron temperature, represented on the right part of the figure 2 and explained in part 2.2, we infer the average electron temperature $\langle T_e \rangle$ of the samples, represented for 30 nm and 100 nm thick copper on the right part of figure 6.

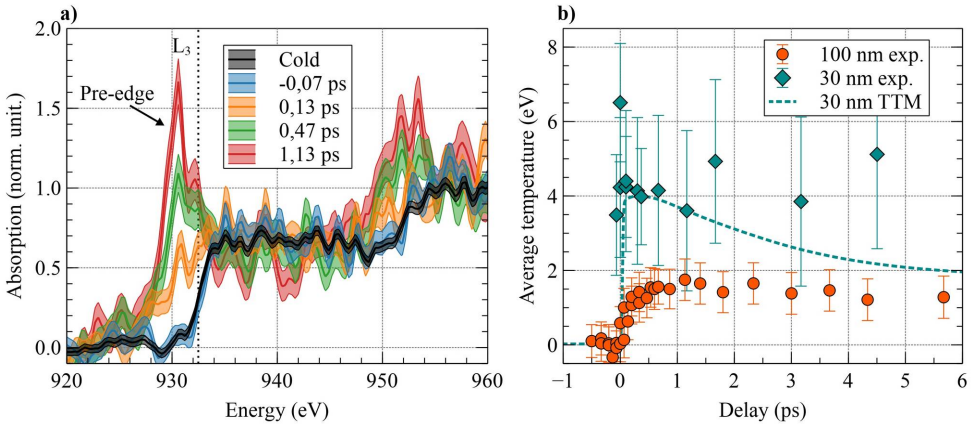

Figure 6. Left: examples of XANES spectra for 100 nm thick copper samples recorded at ambient ("cold") and four different delays before and after the heating. Cold (black) spectrum is averaged over 1000 shots. Uncertainty from the photon counting statistics is represented by the colored areas around each plot. Right: time evolution of the average temperature measured for 30 nm (blue diamonds) and 100 nm thick samples (orange circles). Hydrodynamics TTM simulation for 30 nm copper and diffusive transport is represented (dotted blue line, see figure 7 for details). The time origin is set to the maximum of the pump pulse.

The first observation is that for 30 nm samples, despite large error bars, $<T_e>$ grows approximately 3 times higher than for the 100 nm samples (~4.5 eV and 1.5 eV respectively). It means that all the energy is deposited within at least 30 nm of copper, and is not lost in the Mylar substrate, or in potential electrons cloud for example [27-29], which is supported by hydrodynamics TTM simulations (see part 3.4). The maximum of $<T_e>$ is reached for the first probed time delay, which support a time resolution better than 75 fs like estimated in previous work [5]. For the 100 nm data, the average electron temperature increases up to 1.5 eV in approximately 1 ps, and decreases slowly on a longer time scale due to electron-ion thermal equilibration [9, 19, 30].

3.4 Two-temperature hydrodynamic simulations and discussion

Hydrodynamics TTM simulations have been conducted to interpret the experimental results. Three *scenarios* have been considered in our simulations. The first scenario models a completely ballistic electron energy transport (BT), where the energy is homogeneously deposited in both 30 nm and 100 nm samples. The second models a completely diffusive energy transport (DT), where all the absorbed energy is concentrated in the skin depth and heat gradually the sample in depth. The third, called "composite transport" (CT), models a saturated ballistic electron transport, where in our case 60% of the energy is transported ballistically through the sample and contribute to a homogeneous heating, and 40% is concentrated within the skin depth. These three *scenarios* are represented in the figure 7, where the electron temperature T_e is represented for the Lagrangian positions in the sample and evolves over time. For the TTM simulations, we used the electron heat capacity C_e and the electron-ion coupling G_{ei} from Lin *et al.* [11] and the electronic thermal conductivity κ_e from Anisimov and Rethfeld [31]. The deduced value of $<T_e>$ is then compared with the experimental data for each scenario, as represented in the figure 8 which is focused on the first picosecond after the heating.

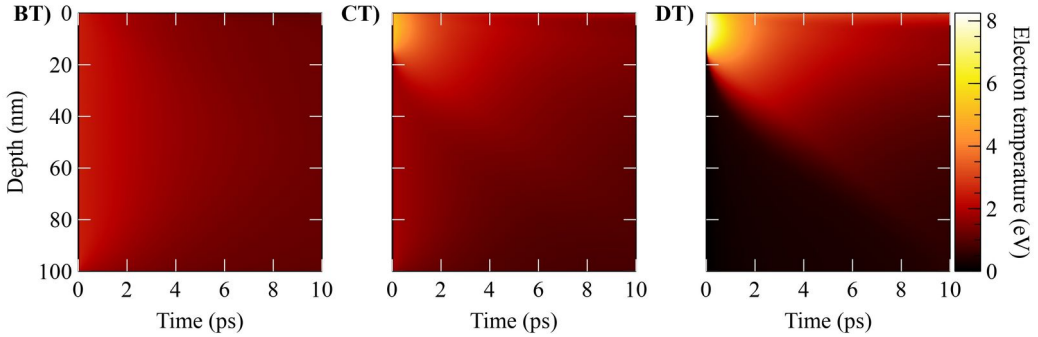

Figure 7. Hydrodynamics TTM simulations for 100 nm copper showing the electron temperature as a function of the Lagrangian position (depth) of the sample and of time for three *scenarios*: BT, CT and DT (details in the text).

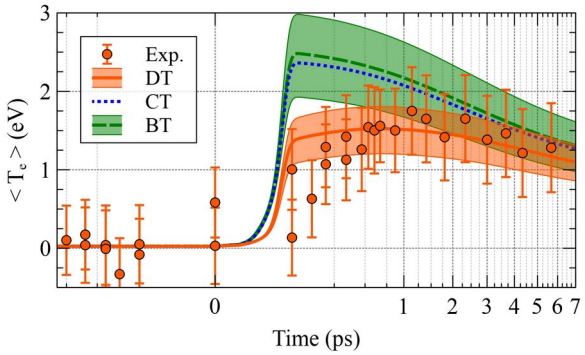

Figure 8. Deduced values of $<T_e>$ from the data of the figure 7 compared to the measurements of T_e for the 100 nm copper sample. The scale of the time axis is cubic to focus on the short times before and after the heating. Experimental uncertainty on the absorbed energy is taken into account in the simulations and represented by the colored areas surrounding calculations. *Figure taken from ref. [8].*

The first observation of the figure 8 is that the experimental data are not reproduced either with the 100% ballistic transport or the composite transport calculations, in terms of maximum temperature reached or the corresponding time. On the contrary, the 100% diffusive transport reproduces well the experimental data. Even if the energy is deposited in few tens of fs, the average electron temperature continues to increase because of the strong T_e dependence of the electron heat capacity C_e. The simulated $<T_e>$ reaches 1.5 ± 0.3 eV in 0.5 – 1 ps in close agreement with the measurements, while the temperature along the 100 nm is strongly heterogeneous. It confirms that the thermal diffusion has taken over the energy transport in this regime above the flux limit for ballistic electrons. Even more, as the composite transport doesn't reproduce the measurements, it seems to indicate that the ballistic component of the transport is greatly reduced, which can be interpreted as a reduction of the ballistic electron range, as suggested by Li *et al.* [28] and Ogitsu *et al.* [32], due to an increase of the electron-electron collision rate with the temperature in the WDM regime [33].

In the often used mJ/cm² flux regime, the hypothesis of thermalized electron population used in the TTM is not acquired [34] in the first moments of the heating process. But in our J/cm² regime, regarding the expected collision rate increase, the corresponding thermalization time is expected to be shorter than 10 fs [35, 36], supporting the use of the TTM to describe our system.

4. CONCLUSION

WDM is a challenging regime to explore, as it requires specific experimental tools to be produced and studied, specially out of equilibrium. It has been made possible thanks to the use of femtosecond lasers which can heat the valence electrons up to few eVs while letting the crystal lattice relatively cold. The study of equilibrium WDM using XANES spectroscopy is easy to perform with standards picosecond plasma x-ray sources, which are good tools as they are bright, with high repetition rate, with a relatively flat and stable spectrum. It allows to study the electronic and atomic structures of the WDM on few picoseconds time-scale, and investigate phase transitions, energy transport and thermodynamical properties of WDM. One of the main limit with the use of laser to produce WDM appears when we want to heat the samples above the flux limit Q_{NT} defined in [23]. Indeed, we need to be sure to produce and probe a homogeneous slab of WDM to infer its physical properties. To the best of our knowledge, the flux investigated in most previous experimental works was below the flux limit, so the saturation of ballistic transport was not an issue (see for example refs. [1, 6, 7, 16, 19-21, 30, 37-40]).

The recent development of the femtosecond betatron x-ray source allowed us to follow the dynamics of the electron temperature in out-of-equilibrium WDM copper, and highlight that the more we heat the sample, the more localized is the heating beneath the surface of the film as the ballistic contribution to the energy transport is strongly reduced. To get homogeneous slabs of WDM with high T_e, it should imply to work with very thin films, of the order of the skin depth, but it would also lead to a strongly decreased signal-to-noise ratio for XANES, so an even more challenging work. Nevertheless, the simultaneous use of *ab initio* and hydrodynamics TTM simulations to interpret time-resolved XANES experiments has been proven to be a powerful study protocol of the laser produced WDM, which can be used to a wide variety of materials, and can now be extended to the femtosecond time-scale thanks to the betatron source.

REFERENCES

[1] Dorchies F. and Recoules V., "Non-equilibrium solid-to-plasma transition dynamics using XANES diagnostic", Physics Reports **657**, 1-26 (2016).

[2] Dorchies F. *et al*., "Unraveling the Solid-Liquid-Vapor Phase Transition Dynamics at the Atomic Level with Ultrafast X-Ray Absorption Near-Edge Spectroscopy", Physical Review Letters **107**, 245006 (2011).

[3] Leguay P. M. *et al*., "Ultrafast Short-Range Disordering of Femtosecond-Laser-Heated Warm Dense Aluminum", Physical Review Letters **111**, 245004 (2013).

[4] Dorchies F. *et al*., "Experimental station for laser-based picosecond time-resolved x-ray absorption near-edge spectroscopy", Review of Scientific Instruments **86**, 073106 (2015).

[5] Mahieu B. *et al*., "Probing warm dense matter using femtosecond X-ray absorption spectroscopy with a laser-produced betatron source", Nature Communications **9**, 3276 (2018).

[6] Jourdain N. *et al*., "Electron-ion thermal equilibration dynamics in femtosecond heated warm dense copper", Physical Review B **97**, 075148 (2018).

[7] Jourdain N. *et al*., "Ultrafast Thermal Melting in Nonequilibrium Warm Dense Copper", Physical Review Letters **126**, 065001 (2021).

[8] Grolleau A. *et al*., "Femtosecond Resolution of the Nonballistic Electron Energy Transport in Warm Dense Copper", Physical Review Letters **127**, 275901 (2021).

[9] Jourdain N. *et al*., "Understanding XANES spectra of two-temperature warm dense copper using *ab initio* simulations", Physical Review B **101**, 125127 (2020).

[10] Anisimov S. I. *et al*., "Electron emission from metal surfaces exposed to ultrashort laser pulses", Sov. Phys. JETP **39**, 375 (1974).

[11] Lin Z. *et al*., "Electron-Phonon Coupling and Electron Heat Capacity of Metals under Conditions of Strong Electron-Phonon Nonequilibrium", Physical Review B **77**, 075133 (2008).

[12] Simoni J. *et al*., "First-Principles Determination of Electron-Ion Couplings in the Warm Dense Matter Regime", Physical Review Letters **122**, 205001 (2019).

[13] Colombier J.-P. *et al*., "Hydrodynamic simulations of metal ablation by femtosecond laser irradiation", Physical Review B **71**, 165406 (2005).

[14] Siders C. W. *et al*., "Detection of Nonthermal Melting by Ultrafast X-ray Diffraction", Science **286**, 1340 (1999).

[15] Recoules V. *et al*., "Effect of Intense Laser Irradiation on the Lattice Stability of Semiconductors and Metals", Physical Review Letters **96**, 055503 (2006).

[16] Ernstorfer R. *et al*., "The Formation of Warm Dense Matter: Experimental Evidence for Electronic Bond Hardening in Gold", Science **323**, 1033 (2009).

[17] Dorchies F. *et al*., "Comparisons of x-ray sources generated from subpicosecond laser-plasma interaction on clusters and on solid targets", Physical Review E **98**, 033212 (2018).

[18] Doepp A. *et al*., "Stable femtosecond X-rays with tunable polarization from a laser-driven accelerator", Light: Science and Applications **6**, e17086 (2017).

[19] Cho B. I. e*t al.*, "Electronic Structure of Warm Dense Copper Studied by Ultrafast X-Ray Absorption Spectroscopy", Physical Review Letters **106**, 167601 (2011)

[20] Mo M. Z. *et al.*, "Heterogeneous to homogeneous melting transition visualized with ultrafast electron diffraction", Science **360**, 1451 (2018)

[21] Widmann K. *et al.*, "Single-State Measurement of Electrical Conductivity of Warm Dense Gold", Physical Review Letters **92**, 125002 (2004)

[22] Ng A. *et al.*, "Idealized slab plasma approach for the study of warm dense matter", Laser and Particle Beams, **23**(4), 527-537 (2005)

[23] Chen Z. *et al.*, "Flux-Limited Nonequilibrium Electron Energy Transport in Warm Dense Gold", Physical Review Letters **108**, 165001 (2012)

[24] Johnson P. B. and Christy R. W., "Optical Constants of the Noble Metals", Physical Review B **6**, 4370 (1972)
[25] Ashcroft N. W. and Mermin N. D., "Solid State Physics", Harcourt College Publishers, New York (1976).
[26] Hohlfeld J. *et al.*, "Electron and lattice dynamics following optical excitation of metals", Chemical Physics **251**, 1-3, 237-258 (2000)
[27] Ping Y. *et al.*, "Warm dense matter created by isochoric laser heating", High Energy Density Physics **6**, 2, 246-257 (2010)
[28] Li J. *et al.,* "Probing the warm dense copper nano-foil with ultrafast electron shadow imaging and deflectometry", High Energy Density Physics **8**, 3, 298-302 (2012)
[29] Daraszewicz S. L. *et al.,* "Structural dynamics of laser-irradiated gold nanofilms", Physical Review B 8**8**, 184101 (2013)
[30] Cho B. I. e*t al.*, "Measurement of Electron-Ion Relaxation in Warm Dense Copper", Scientific Reports **6**, 18843 (2016)
[31] Anisimov S. I. and Rethfeld B.,"Theory of ultrashort laser pulse interaction with a metal" Proc. SPIE **3093**, Nonresonant Laser-Matter Interaction (NLMI-9), (1997).
[32] Ogitsu T. *et al.*, "Ballistic electron transport in non-equilibrium warm dense gold", High Energy Density Physics **8**, 3, 303-306 (2012)
[33] Fourment C. *et al.*, "Experimental determination of temperature-dependent electron-electron collision frequency in isochorically heated warm dense gold", Physical Review B **89**, 161110(R) (2014)
[34] Obergfell M. and Demsar J., "Tracking the Time Evolution of the Electron Distribution Function in Copper by Femtosecond Broadband Optical Spectroscopy", Physical Review Letters **124**, 037401 (2020)
[35] Mueller B. Y. and Rethfled B., "Relaxation dynamics in laser-excited metals under nonequilibrium conditions", Physical Review B **87**, 035139 (2013)
[36] Chang H. T. *et al.*, "Electron thermalization and relaxation in laser-heated nickel by few-femtosecond core-level transient absorption spectroscopy", Physical Review B **103**, 064305 (2021)
[37] Chen Z. *et al.*, "Evolution of ac Conductivity in Nonequilibrium Warm Dense Gold", Physical Review Letters **110**, 135001 (2013)
[38] Chen Z. *et al.*, "Interatomic Potential in the Nonequilibrium Warm Dense Matter Regime", Physical Review Letters **121**, 075002 (2018)
[39] Ao T. *et al.*, "Optical Properties in Nonequilibrium Phase Transitions", Physical Review Letters **96**, 055001 (2006)
[40] Siwick B. J. *et al.*, "An Atomic-Level View of Melting Using Femtosecond Electron Diffraction", Science **302**, 1382 (2003)